Biomedical Optics EXPRESS

Spatial characterization of corneal biomechanical properties with optical coherence elastography after UV cross-linking

Michael D. Twa,[1,2,*] Jiasong Li,[2] Srilatha Vantipalli,[1] Manmohan Singh,[2] Salavat Aglyamov,[3] Stanislav Emelianov,[3] and Kirill V. Larin[2,4]

[1] *University of Houston, College of Optometry, 505 J. Davis Armistead Building, Houston, Texas 77204-2020, USA*
[2] *University of Houston, Department of Biomedical Engineering, 4800 Calhoun Road, Houston, Texas 77004, USA*
[3] *The University of Texas at Austin, Department of Biomedical Engineering, 107 W. Dean Keeton Street Stop C0800, Austin, Texas 78712, USA*
[4] *Baylor College of Medicine, Department of Molecular Physiology and Biophysics, One Baylor Plaza, Houston, Texas 77030, USA*
[*] *mtwa@optometry.uh.edu*

Abstract: Corneal collagen cross-linking (CXL) is a clinical treatment for keratoconus that structurally reinforces degenerating ocular tissue, thereby limiting disease progression. Clinical outcomes would benefit from noninvasive methods to assess tissue material properties in affected individuals. Regional variations in tissue properties were quantified before and after CXL in rabbit eyes using optical coherence elastography (OCE) imaging. Low-amplitude (<1μm) elastic waves were generated using micro air-pulse stimulation and the resulting wave amplitude and speed were measured using phase-stabilized swept-source OCE. OCE imaging following CXL treatment demonstrates increased corneal stiffness through faster elastic wave propagation speeds and lower wave amplitudes.

OCIS codes: (170.0170) Medical optics and biotechnology; (110.4500) Optical coherence tomography; (170.4580) Optical diagnostics for medicine; (170.6935) Tissue characterization.

References and links

1. A. Sarvazyan, T. J. Hall, M. W. Urban, M. Fatemi, S. R. Aglyamov, and B. S. Garra, "An Overview of Elastography - an Emerging Branch of Medical Imaging," Curr. Med. Imaging Rev. **7**(4), 255–282 (2011).
2. T. B. Edrington, K. Zadnik, and J. T. Barr, "Keratoconus," Optom. Clin. **4**(3), 65–73 (1995).
3. M. D. Twa, J. J. Nichols, C. E. Joslin, P. S. Kollbaum, T. B. Edrington, M. A. Bullimore, G. L. Mitchell, K. J. Cruickshanks, and D. J. Schanzlin, "Characteristics of corneal ectasia after LASIK for myopia," Cornea **23**(5), 447–457 (2004).
4. K. Zadnik, J. T. Barr, T. B. Edrington, D. F. Everett, M. Jameson, T. T. McMahon, J. A. Shin, J. L. Sterling, H. Wagner, and M. O. Gordon, "Baseline findings in the Collaborative Longitudinal Evaluation of Keratoconus (CLEK) Study," Invest. Ophthalmol. Vis. Sci. **39**(13), 2537–2546 (1998).
5. H. Latorre-Ossa, J. L. Gennisson, E. De Brosses, and M. Tanter, "Quantitative imaging of nonlinear shear modulus by combining static elastography and shear wave elastography," IEEE Trans. Ultrason. Ferroelectr. Freq. Control **59**(4), 833–839 (2012).
6. D. Touboul, J. L. Gennisson, T. M. Nguyen, A. Robinet, C. J. Roberts, M. Tanter, and N. Grenier, "Supersonic shear wave elastography for the in vivo evaluation of trans-epithelial corneal collagen cross-linking," Invest. Ophthalmol. Vis. Sci. **55**(3), 1976–1984 (2014).
7. J. D. Kovač, M. Daković, D. Stanisavljević, T. Alempijević, R. Ješić, P. Seferović, and R. Maksimović, "Diffusion-weighted MRI versus transient elastography in quantification of liver fibrosis in patients with chronic cholestatic liver diseases," Eur. J. Radiol. **81**(10), 2500–2506 (2012).
8. G. Scarcelli, R. Pineda, and S. H. Yun, "Brillouin optical microscopy for corneal biomechanics," Invest. Ophthalmol. Vis. Sci. **53**(1), 185–190 (2012).
9. B. F. Kennedy, M. Wojtkowski, M. Szkulmowski, K. M. Kennedy, K. Karnowski, and D. D. Sampson, "Improved measurement of vibration amplitude in dynamic optical coherence elastography," Biomed. Opt. Express **3**(12), 3138–3152 (2012).
10. K. M. Kennedy, B. F. Kennedy, R. A. McLaughlin, and D. D. Sampson, "Needle optical coherence elastography for tissue boundary detection," Opt. Lett. **37**(12), 2310–2312 (2012).

#204792 - $15.00 USD Received 17 Jan 2014; revised 28 Mar 2014; accepted 31 Mar 2014; published 4 Apr 2014

11. M. Razani, A. Mariampillai, C. Sun, T. W. Luk, V. X. Yang, and M. C. Kolios, "Feasibility of optical coherence elastography measurements of shear wave propagation in homogeneous tissue equivalent phantoms," Biomed. Opt. Express **3**(5), 972–980 (2012).
12. B. F. Kennedy, T. R. Hillman, R. A. McLaughlin, B. C. Quirk, and D. D. Sampson, "In vivo dynamic optical coherence elastography using a ring actuator," Opt. Express **17**(24), 21762–21772 (2009).
13. C. Li, G. Guan, X. Cheng, Z. Huang, and R. K. Wang, "Quantitative elastography provided by surface acoustic waves measured by phase-sensitive optical coherence tomography," Opt. Lett. **37**(4), 722–724 (2012).
14. J. Schmitt, "OCT elastography: imaging microscopic deformation and strain of tissue," Opt. Express **3**(6), 199–211 (1998).
15. M. R. Ford, W. J. Dupps, Jr., A. M. Rollins, A. S. Roy, and Z. Hu, "Method for optical coherence elastography of the cornea," J. Biomed. Opt. **16**(1), 016005 (2011).
16. R. K. Manapuram, S. A. Baranov, V. G. R. Manne, N. Sudheendran, M. Mashiatulla, S. Aglyamov, S. Emelianov, and K. V. Larin, "Assessment of wave propagation on surfaces of crystalline lens with phase sensitive optical coherence tomography," Laser Phys. Lett. **8**(2), 164–168 (2011).
17. H. Wang, P. L. Prendiville, P. J. McDonnell, and W. V. Chang, "An ultrasonic technique for the measurement of the elastic moduli of human cornea," J. Biomech. **29**(12), 1633–1636 (1996).
18. S. A. Greenstein, K. L. Fry, and P. S. Hersh, "In vivo biomechanical changes after corneal collagen cross-linking for keratoconus and corneal ectasia: 1-year analysis of a randomized, controlled, clinical trial," Cornea **31**(1), 21–25 (2012).
19. Y. Hon and A. K. Lam, "Corneal deformation measurement using Scheimpflug noncontact tonometry," Optom. Vis. Sci. **90**(1), e1–e8 (2013).
20. D. Alonso-Caneiro, K. Karnowski, B. J. Kaluzny, A. Kowalczyk, and M. Wojtkowski, "Assessment of corneal dynamics with high-speed swept source optical coherence tomography combined with an air puff system," Opt. Express **19**(15), 14188–14199 (2011).
21. C. Dorronsoro, D. Pascual, P. Pérez-Merino, S. Kling, and S. Marcos, "Dynamic OCT measurement of corneal deformation by an air puff in normal and cross-linked corneas," Biomed. Opt. Express **3**(3), 473–487 (2012).
22. S. Wang, K. V. Larin, J. Li, S. Vantipalli, R. K. Manapuram, S. Aglyamov, S. Emelianov, and M. D. Twa, "A focused air-pulse system for optical-coherence-tomography-based measurements of tissue elasticity," Laser Phys. Lett. **10**(7), 075605 (2013).
23. S. Wang, J. Li, R. K. Manapuram, F. M. Menodiado, D. R. Ingram, M. D. Twa, A. J. Lazar, D. C. Lev, R. E. Pollock, and K. V. Larin, "Noncontact measurement of elasticity for the detection of soft-tissue tumors using phase-sensitive optical coherence tomography combined with a focused air-puff system," Opt. Lett. **37**(24), 5184–5186 (2012).
24. R. K. Manapuram, V. G. R. Manne, and K. V. Larin, "Development of phase-stabilized swept-source OCT for the ultrasensitive quantification of microbubbles," LaPhy **18**, 1080–1086 (2008).
25. J. Li, S. Wang, R. K. Manapuram, M. Singh, F. M. Menodiado, S. Aglyamov, S. Emelianov, M. D. Twa, and K. V. Larin, "Dynamic optical coherence tomography measurements of elastic wave propagation in tissue-mimicking phantoms and mouse cornea in vivo," J. Biomed. Opt. **18**(12), 121503 (2013).
26. M. Hovakimyan, R. Guthoff, S. Knappe, A. Zhivov, A. Wree, A. Krüger, A. Heisterkamp, and O. Stachs, "Short-term corneal response to cross-linking in rabbit eyes assessed by in vivo confocal laser scanning microscopy and histology," Cornea **30**(2), 196–203 (2011).
27. S. Kling, L. Remon, A. Pérez-Escudero, J. Merayo-Lloves, and S. Marcos, "Corneal biomechanical changes after collagen cross-linking from porcine eye inflation experiments," Invest. Ophthalmol. Vis. Sci. **51**(8), 3961–3968 (2010).
28. S. Schumacher, L. Oeftiger, and M. Mrochen, "Equivalence of biomechanical changes induced by rapid and standard corneal cross-linking, using riboflavin and ultraviolet radiation," Invest. Ophthalmol. Vis. Sci. **52**(12), 9048–9052 (2011).
29. G. Wollensak, E. Spoerl, and T. Seiler, "Stress-strain measurements of human and porcine corneas after riboflavin-ultraviolet-A-induced cross-linking," J. Cataract Refract. Surg. **29**(9), 1780–1785 (2003).
30. S. Kling, H. Ginis, and S. Marcos, "Corneal biomechanical properties from two-dimensional corneal flap extensiometry: application to UV-riboflavin cross-linking," Invest. Ophthalmol. Vis. Sci. **53**(8), 5010–5015 (2012).
31. A. Sinha Roy, K. M. Rocha, J. B. Randleman, R. D. Stulting, and W. J. Dupps, Jr., "Inverse computational analysis of in vivo corneal elastic modulus change after collagen crosslinking for keratoconus," Exp. Eye Res. **113**, 92–104 (2013).

1. Introduction

The biomechanical properties of a tissue are often altered by disease and in some cases these structural changes are the basis for early detection of tissue abnormalities [1]. Non-invasive measurements of ocular tissue biomechanical properties *in vivo* remain a challenging problem due the structural complexity and the delicate nature of most ocular tissues.

Keratoconus is a structural degeneration of the eye characterized by localized corneal thinning and vision impairment that often leads to corneal transplant. The current diagnostic

#204792 - $15.00 USD Received 17 Jan 2014; revised 28 Mar 2014; accepted 31 Mar 2014; published 4 Apr 2014

hallmarks for this condition are based upon detecting characteristic patterns of localized morphologic corneal distortion secondary to the underlying structural degeneration [2–4]. UV-induced corneal collagen cross-linking (CXL) is a relatively new clinical treatment for keratoconus that is intended to modify the material properties of diseased corneal tissue, increasing corneal stiffness and thereby deferring further degeneration or more invasive surgical treatments. The mechanism by which CXL stiffens the corneal tissue is not fully understood and, at present, treatments are fairly uniform despite individual disease presentation or severity.

The purpose of this study is to assess the feasibility of using an optical coherence tomography-based imaging technique, optical coherence elastography (OCE) to quantify local spatial variations in corneal tissue properties induced by CXL treatment. If structural compromise of corneal tissue precedes the gross clinical manifestations of keratoconus, then the ability to quantify regional structural properties of corneal tissue *in vivo* may be useful for early disease detection, as well as provide guidance for the timing and selection of CXL treatments.

A number of other methods have been developed to quantify the elastic properties of soft tissues such as ultrasound [5, 6], MRI [7], Brillouin scattering [8], and more recently, optical coherence tomography imaging [9–15]. Elasticity imaging consists of baseline structural imaging followed by mechanical tissue stimulation (e.g. low frequency ultrasound pulse, air impulse, etc.) to induce tissue deformation, and re-imaging to capture the resulting deformation response. Biomechanical properties such as the elastic modulus can then be derived from quantitative image analysis using appropriate mathematical modeling techniques. While the above methods are non-invasive, Optical Coherence Tomography (OCT)-based elasticity imaging has the advantage of high spatial and temporal resolution. Phase-resolved imaging methods based on processing the complex component of the OCT signal enable sub-micron resolution that is sufficient to detect micron and sub-micron-level dynamic phenomena. This sensitivity is beyond the capability of ultrasound and MRI-based imaging techniques, and even conventional clinical OCT imaging. However, this high spatiotemporal resolution is sufficient to resolve the structural effects of corneal disease [13, 16, 17].

Existing methods to measure the biomechanical properties of corneal tissue (Ocular Response Analyzer; Reichert Technologies, Depew, NY and Corvis ST; Oculus Inc., Arlington, WA) are based upon a high volume, long duration air pulse [18, 19]. Although non-invasive, such measurements are potentially confounded by biomechanical responses from surrounding tissues [20, 21]. The large tissue deformation responses produced, displace aqueous fluid within the anterior chamber, cause movement of the iris and lens, and movement of the eye into the orbit. In keratoconus, the cornea is typically affected in discrete regions–usually inferiorly. Therefore, the capability to distinguish regional differences in corneal tissue properties is important for disease detection and monitoring the effects of treatment. In theory, elastography methods that apply a smaller load to the cornea, with tissue excitation over a small area may better detect local variations in structural properties.

To address these current challenges, we developed a micro air-pulse stimulator (MAPS) to produce spatiotemporally discrete tissue excitation that is synchronized with a high resolution phase-sensitive OCT imaging system [22]. Together, these components provide a platform for optical coherence elastography imaging capable of high spatial and temporal imaging resolution as well as focused tissue excitation that is isolated to the tissue of interest [23]. This elastography imaging system was used to quantify the amplitude and velocity of microscopic elastic waves generated in rabbit corneal tissues that were subjected to UV-riboflavin induced collagen cross-linking treatments. The elastography results were then compared with measurements of Young's modulus from conventional mechanical extensiometry.

#204792 - $15.00 USD Received 17 Jan 2014; revised 28 Mar 2014; accepted 31 Mar 2014; published 4 Apr 2014

2. Experimental methods

2.1 Optical coherence elastography imaging system configuration

A schematic layout of the OCE system is shown in Fig. 1. The imaging subsystem is a phase stabilized swept source OCT. The laser source (HSL2000, Santec, Inc., Torrance, California) has a central wavelength of 1310 ± 75 nm, A-scan rate of 30 kHz, and output power of 36 mW. Additional details of this imaging system can be found in our previous publications [24]. The laser source is split (99/1) with 99% to the imaging interferometer that contains reference and sample arms. Fringes are formed from interference of light returned from each of the arms, which is then detected by a balanced photodetector (PDB130C, Thorlabs). The CPU acquires data by digitizing the photodetector output using a 16-bit analog to digital converter (ADC; ATS9462, AlazarTech). The remaining 1% of light from the laser is fed to a fiber Bragg grating which returns a synchronizing pulse every time it scans the central wavelength (30 kHz); this pulse triggers the ADC. Because the trigger signal follows the laser, synchronization errors between the source and the data acquisition are minimized providing high phase stability [25]. During these tissue experiments, the measured standard deviation of phase stability was 41 rad (85 nm), which determined the lower limit of detection for tissue surface displacement. The sample interrogation path includes a pair of mirror galvanometers and a scan lens objective that provides a lateral resolution of 10 µm. This system is linked to the CPU for signal processing and image formation.

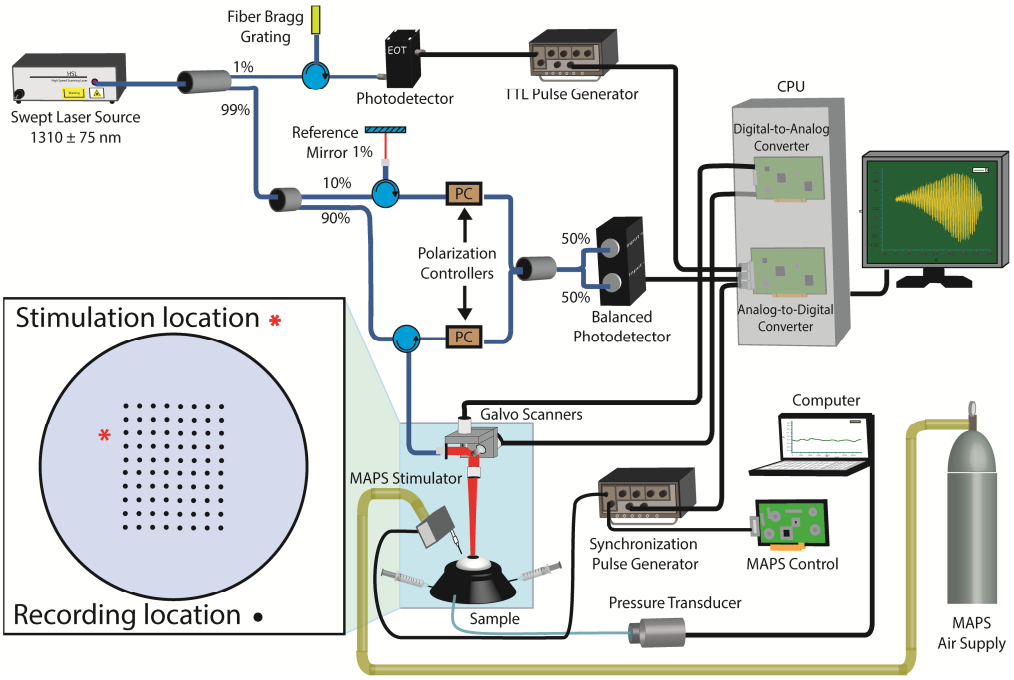

Fig. 1. Phase-sensitive optical coherence tomography-based elastography imaging system comprised of a swept-source laser OCT imaging subsystem and a synchronized micro air pulse tissue stimulator (MAPS system). Inset shows the location of sample stimulation (*) relative to the recording positions (•)

The Micro Air Pulse Stimulator (MAPS) subsystem depicted in Fig. 1 produces discrete tissue stimulation through an electromechanically gated high-speed solenoid valve. The MAPS controller also synchronizes with the imaging subsystem and initiates image capture. Tissue stimulation delivered by the MAPS subsystem produces a controlled air pulse with a Gaussian spatiotemporal profile (FWHM = 2.4 Pa or 3.5 x10^{-4} psi, 800 µs duration, 150 µm

#204792 - $15.00 USD Received 17 Jan 2014; revised 28 Mar 2014; accepted 31 Mar 2014; published 4 Apr 2014

diameter). This pulse can be configured to permit higher pressure, longer duration, and positioned to stimulate the tissue at a variety of locations, distances and angles of incidence.

2.2 Tissue preparation and elastography imaging

Whole eyes from New Zealand white rabbits were obtained frozen from Pel-Freeze Biologicals (Rogers, AR). Tissues were thawed and irrigated every 2 minutes with a balanced salt solution. Considerable care was taken to position each eye using the corneal apex as a reference point to center a grid of OCE measurement locations. Prior to elastography imaging, samples were examined to determine anatomical orientation and gentian violet ink marks were placed at the superior and nasal limbus to help maintain orientation throughout the experiments. Samples were then placed in a custom eye holder and the rotational position of the globe was orthogonally fixed (X and Y axes) with two 23-gauge needles placed near the equator such that the geometric center of the cornea was centered and oriented normal to the horizontal plane. Intraocular pressure of the sample was monitored throughout the experiment using an analog pressure transducer (model 41X; Keller instruments) and pressure was maintained at physiological levels (15 mm Hg) by a computer controlled micro-infusion pump.

Tissue cross-linking treatment was performed by first removing the corneal epithelium using a blunt surgical spatula. A 0.1% riboflavin solution in 0.9% phosphate buffered saline without Dextran was applied to the bare stromal surface and allowed to penetrate with re-application at 5 min intervals for a total of 30 minutes. The cornea was then irradiated with a non-proprietary UV light source (365 nm; 7 mm diameter, 3 mW/cm^2 for 30 min) to induce tissue cross-linking. During irradiation, the riboflavin solution was reapplied every 5 minutes. Samples were positioned for elasticity imaging immediately following cross-linking treatments. Elastography measurements were completed within 15 minutes of CXL treatment.

A 3D-linear micrometer stage was used to laterally align the corneal apex to the imaging axis for elastography measurements. The OCE sampling grid (4x5 mm; 550 μm sample spacing) was centered relative to the corneal apex and the air-pulse stimulator positioned approximately 1 mm beyond the sampling grid (2.5 mm lateral to the corneal apex) to avoid near-field effects of tissue stimulation (Fig. 1 inset). Air pulse tissue stimulation (2.4 Pa) was performed approximately 400 μm from the tissue surface with the force directed normal to the cornea (Fig. 1). This same tissue stimulation and response measurement geometry was performed for both untreated and cross-linked tissue.

Each stimulation event generated corneal tissue deformation. We describe these deformations as elastic wave propagation in the cornea using a Lamb wave model. This model is based on full thickness deformation of a thin plate and is typically used to describe the propagation of flexural waves in plates. We consider this physical model as a first-order approximation of the elastic wave propagation in the cornea. Wave amplitude was calculated from the measured phase displacement relative to the original state using Eq. (1):

$$Amplitude = (\lambda / 2\pi) \times phase, \tag{1}$$

where λ is the central wavelength of the OCE system (1310 nm). Wave amplitude was sequentially measured at each response location (Fig. 1 inset) while a constant stimulation position was maintained throughout measurements. Corneal tissue properties are heterogeneous, both laterally and by depth. The biomechanical responses measured in this study reflect the sum of biomechanical properties integrated across the full thickness of the cornea. Results are presented as the mean of multiple measurements (n = 10) obtained at each response location and averaged across multiple samples. Interpolation between the aligned sample points was performed using two-dimensional bi-linear interpolation (Matlab, Mathworks, Natick, MA). A total of 4 eyes were measured before and after CXL treatments. Spatial maps of surface wave amplitude by location were generated from the average of all samples (n = 4 in each treatment group). The difference in elastic wave amplitude between

#204792 - $15.00 USD Received 17 Jan 2014; revised 28 Mar 2014; accepted 31 Mar 2014; published 4 Apr 2014

normal and CXL treated samples was summarized by calculating the average amplitude for each of the three nearest-neighbor recording locations closest to the point of stimulation.

Elastic wave propagation speed was calculated relative to a common reference point–the measurement point closest to the point of tissue stimulation, which was on average ~1 mm separation. The time delay for elastic wave propagation between the reference point and each measurement location was recorded. A 2-D surface plot of this temporal delay was generated from the average response at each recording position. The difference in elastic wave propagation velocity for normal and CXL treated samples was calculated from the average time delay observed between the reference point and each of the nearest-neighboring points. Elastic wave propagation velocity v was calculated as: ($v = d/t$) where d is the distance between sampling locations and t is the observed time delay between measurement points.

2.3 Mechanical testing

Following elastography measurements, central corneal tissue was cut into 7 mm wide by 14 mm long uniform strips and the thickness was measured. Scleral rim tissue was used to grip these samples, which were then tested under mechanical tension using an Instron tester (In-Spec 2200, Instron Inc., Nrowood, MA) with a 125 N load cell. Tissue strips were pre-stressed by placing samples under slight tension and then tested to a strain of approximately 7% elongation. Young's modulus was estimated from the linear portion of the stress-strain curve and results of these experiments were compared with treated and untreated tissue samples.

3. Results and discussion

3.1 Elastic wave amplitude and velocity

Total tissue thickness at the corneal apex was determined from OCT images in untreated samples (735 μm) and in CXL treated samples (615μm). The magnitude of elastic wave amplitude in untreated corneal tissue ranged from approximately 0.5 to 12 μm at the measured location nearest to the point of stimulation (Fig. 2(A)). In cross-linked corneal tissue, elastic wave amplitude was less than untreated tissue, ranging in amplitude from 1.25 μm near the point of excitation to less than 0.5 μm over most of the measured area (Fig. 2(B)). Wave amplitude was smaller in treated tissue and this made it impossible to track wave amplitude and velocity beyond 1-1.5 mm using the same tissue stimulation force before and after CXL treatment. When normalized for maximum amplitude across samples there was on average a 56% decrease in elastic wave amplitude after CXL treatment. Elastic wave amplitude decreased monotonically as a function of distance from the excitation point and this was more pronounced after CXL treatment (Fig. 2(A)-2(B)).

Elastic wave propagation speed was measured by observing the time delay between tissue stimulation and wave detection at each recording position. In untreated tissue (Fig. 2(C)) the time delay increased monotonically as a function of distance from the excitation point. After cross-linking treatments, elastic wave propagation speed was greater than untreated tissues, but difficult to observe over distances greater than 1.5 mm using the same tissue excitation force as was used in normal tissues. To better observe the effects of CXL treatment, we applied a greater tissue stimulation force (4.8 Pa) to a cross-linked sample (n = 1; Fig. 3). We observed a circularly symmetric region within the treated tissue demarcated by low amplitude higher velocity elastic waves. Cross-linked corneal tissues had a more homogenous central zone that corresponded to the area of treatment (Fig. 3).

3.2 Measurement of Young's modulus

Young's modulus was estimated for treated and untreated strips of corneal tissue (n = 4 each) taken from the central corneal region. As shown in Fig. 4, CXL treated tissues had a greater Young's modulus (2.6 MPa) than untreated tissue (1.5 MPa). Although these longitudinal

#204792 - $15.00 USD Received 17 Jan 2014; revised 28 Mar 2014; accepted 31 Mar 2014; published 4 Apr 2014

strip extensiometry measurements do correlate with shear wave elastography observations, it is important to recognize that they evaluate orthogonal material properties that are only directly linked for isotropic homogenous materials. Nevertheless, these strip extensiometry observations do provide comparative data for elastography imaging and previous studies.

A possible limitation of this study is related to averaging responses across samples. The motive behind averaging these samples was to demonstrate the dominant response as well as overall statistical variation due to tissue stimulation. Indeed, one must be careful comparing results across samples as the biomechanical properties may differ. Nevertheless, the experimental results shown in Fig. 2 faithfully represent the monotonic trends observed in

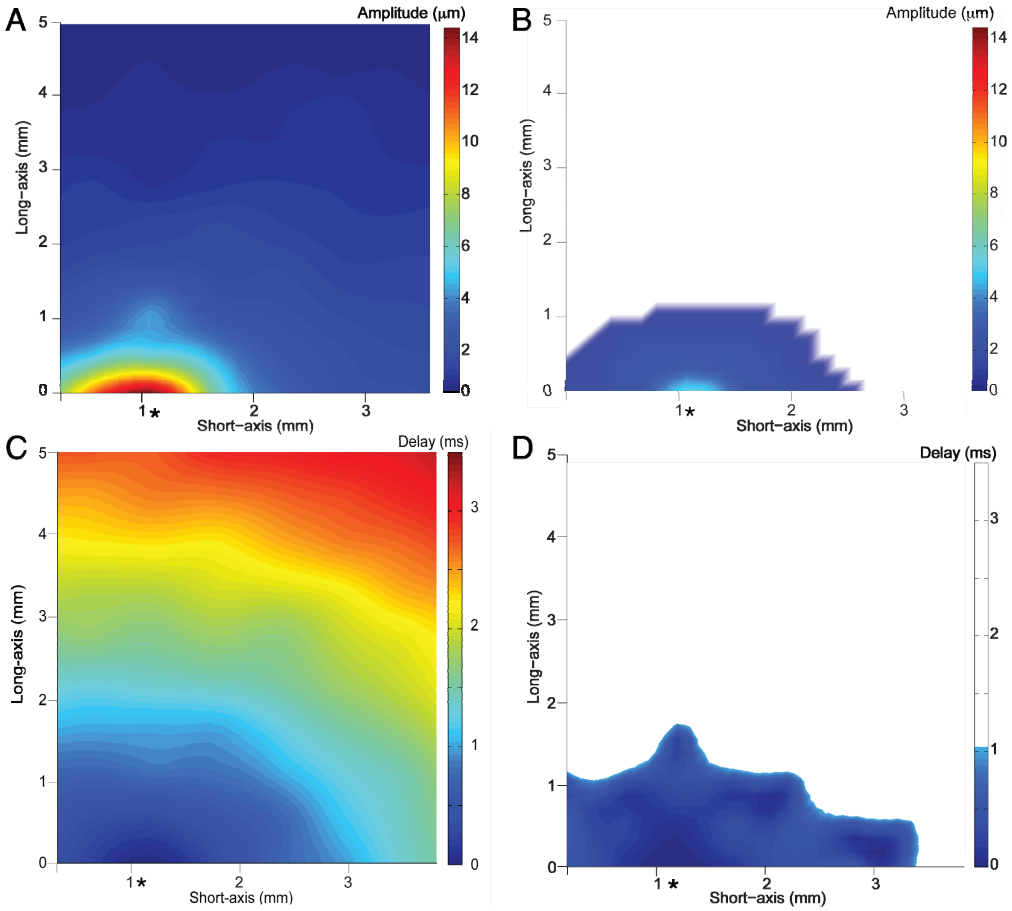

Fig. 2. Corneal tissue response to air pulse stimulation with and without cross-linking treatment. Symbol (*) indicates the approximate location of tissue stimulation. Surface wave amplitude in untreated corneal tissue (A) and after UV cross-linking (B); corneal surface wave amplitude was reduced in treated tissue and could not be measured beyond ~1 mm. Temporal delay observed between tissue surface stimulation and observed surface displacement. Surface wave propagation speed was slower in un-treated tissue as indicated by greater delay times shown by red-shifted colors (C) when compared to tissue after UV cross-linking (D). Note that the time-delay color scales (panels C and D) are the same, but truncated in D where it was not possible to observe surface waves. Lower surface wave amplitude and faster propagation speeds (shorter delay times) are consistent with higher material stiffness.

#204792 - $15.00 USD Received 17 Jan 2014; revised 28 Mar 2014; accepted 31 Mar 2014; published 4 Apr 2014

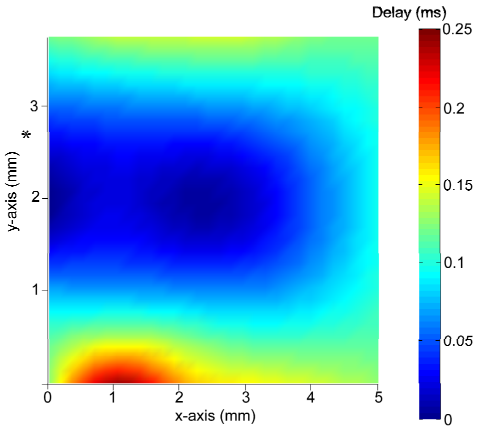

Fig. 3. Elastic wave propagation speed by OCE in the rabbit cornea after CXL. Using a greater tissue stimulation force, it is possible to determine elastic wave propagation over the entire recording surface even in tissue that was made stiffer by the cross-linking treatment. Blue-shifted colors represent shorter time delay between measured points, corresponding to greater elastic wave propagation speed. (*) = point of tissue stimulation (n = 1).

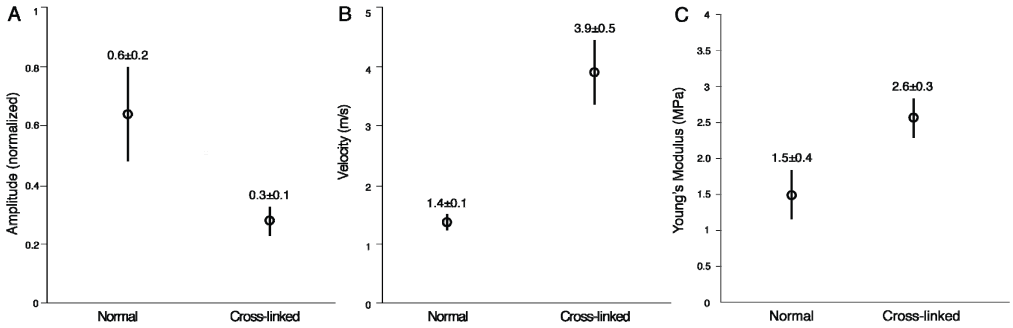

Fig. 4. Comparison of rabbit corneal tissue properties from elastography imaging and mechanical extensiometry measurements before and after cross-linking treatment (n = 4). (A) Comparison of elastic wave amplitude normalized to maximum amplitude. (B) Elastic wave propagation velocity in untreated and cross-linked corneal tissue. (C) Estimation of Young's modulus of the rabbit cornea from mechanical extensiometry measurements of central tissue strips; error bars represent ± one standard deviation.

wave amplitude and propagation speed due to tissue stimulation. While the animals were from approximately the same age group, we acknowledge that the eyes could have different biomechanical properties. Pre-selecting samples with identical structural properties would be ideal, but this assumes that an established non-invasive, non-destructive measurement standard is available to do this. To the best of our knowledge, no such established standard exists and developing this capability is the broader topic of this research.

4. Summary

We demonstrated that elastic waves induced using a controlled micro-air pulse stimulator provide a non-invasive method to produce spatially discrete microscopic tissue deformation that is suitable for elastography measurements in the rabbit cornea before and after CXL treatment. In addition, these results show that using dynamic OCE, it is possible to measure the amplitude and propagation speed of sub-micron mechanical waves over a broad area of corneal tissue, which will be important for clinical diagnostic use. These measurements of dynamic tissue response to micro-air pulse stimulation also correlate with conventional measurements of tissue properties obtained from mechanical tension testing. Finally, we

#204792 - $15.00 USD Received 17 Jan 2014; revised 28 Mar 2014; accepted 31 Mar 2014; published 4 Apr 2014

demonstrated the capability to measure spatial variations in material properties for both normal and CXL treated tissues in the rabbit eye. The ability to determine spatial variations and individual properties is an important prerequisite for optimizing clinical treatments.

These results show that elastic wave amplitude was decreased and that the velocity of elastic wave propagation was greater following CXL treatment, consistent with an increase in material stiffness (Fig. 4). These results are in agreement with others who have used inflation, mechanical extension, and finite element modeling methods to quantify changes in corneal material properties after CXL treatment [26–29]. Using a modified air-puff tonometer that produced global corneal deformation, Dorronsoro and colleagues showed that CXL results in dynamic deformations with smaller diameter and smaller maximum amplitude than untreated tissues, consistent with our results. However, they did not attempt to derive estimates of Young's modulus or compare this method with extensiometry or inflation experiments [21]. Using inflation experiments, Kling and colleagues evaluated rabbit and porcine corneal tissues after CXL and found that Young's modulus increased by a factor of 1.6 to 2.4 [27, 30]. This is similar to the 1.7-fold increase reported here using strip extensiometry. Moreover, it is consistent with the observed 2.0-fold decrease in wave amplitude and 2.7-fold increase in wave propagation velocity, while also providing additional details about the spatial variation in tissue properties.

The increase in Young's modulus observed in this study (1 MPa) is in agreement with computational estimates by Roy and colleagues who predicted a doubling in corneal modulus after corneal cross-linking using a finite element modeling approach [31]. The observed difference in elastic wave propagation velocity was several times greater in CXL treated tissue than in the untreated cornea, Fig. 4. Quantitative modeling of these elastography phenomena and their relationship to fundamental material properties of corneal tissue is the focus of ongoing work.

It appears from these results that treatment effects dominate the observed tissue response with these elastography methods. Corneal tissue is both anisotropic and inhomogeneous. Additional study and optimization of OCE methods is needed to understand how normal and diseased corneal ultrastructure may influence OCE measurements.

4. Conclusion

Phase-sensitive optical coherence elastography has the capability to resolve sub-micron mechanical wave propagation in corneal tissues. Differences in wave amplitude and propagation speed induced by CXL treatments correlate with the observed changes in tissue properties using conventional measurements of material elasticity. Optical coherence elastography appears promising as a technique to quantify the biomechanical properties of corneal tissue in vivo and may be important tool for optimizing clinical treatments.

Acknowledgments

This study was supported by NIH/NEI 1R01EY022362 and P30EY07551.

#204792 - $15.00 USD Received 17 Jan 2014; revised 28 Mar 2014; accepted 31 Mar 2014; published 4 Apr 2014